1986PASJ...38..731S

Publ. Astron. Soc. Japan 38, 731–750 (1986)

X-Ray Probing of the Circumstellar Matter in the Vela X-1 System from Observations over an Eclipse Phase

Naohisa SATO,* Satio HAYAKAWA, and Fumiaki NAGASE

Department of Astrophysics, Faculty of Science, Nagoya University, Furo-cho, Chikusa-ku, Nagoya 464

Kuniaki MASAI

Institute of Plasma Physics, Nagoya University, Furo-cho, Chikusa-ku, Nagoya 464

and

Tadayasu DOTANI, Hajime INOUE, Fumiyoshi MAKINO, Kazuo MAKISHIMA,† and Takaya OHASHI†

Institute of Space and Astronautical Science, 6–1, Komaba 4-chome, Meguro-ku, Tokyo 153

(Received 1986 February 21; accepted 1986 May 21)

Abstract

The X-ray binary pulsar Vela X-1 (4U 0900−403) was observed with the Tenma satellite throughout an entire eclipse in March 1984. The iron emission line at 6.4 keV was observed during the eclipse of Vela X-1 with the intensity of about 15% of that during the noneclipse phase, in contrast to the 2% residual flux of continuum X-rays in the range 2–20 keV. We estimated the scale height of the atmosphere of the companion star HD 77581 to be $\sim 3\times 10^{11}$ cm from the spectral analysis of the data during the emersion of Vela X-1. This scale height can be explained by a hydrostatic model with a strong radiation pressure. Diminishing pulse amplitudes during the ingress and the egress of Vela X-1 also support the existence of an extended stellar atmosphere. The orbital phase dependence of the iron line intensity can be interpreted in terms of the fluorescence emission from the companion atmosphere, the stellar wind, and the matter in the proximity ($\lesssim 3\times 10^{11}$ cm) of the neutron star. The three reprocessing sites contribute about equally to the iron fluorescence line.

Key words: Stellar atmospheres; Stellar winds; Vela X-1; X-ray binaries; X-ray pulsars; X-ray sources; X-ray spectra.

* Present address: Spacecraft and Equipment Design Department, Komukai Works, Toshiba Co., 1, Komukai, Toshiba-cho, Saiwai-ku, Kawasaki 210.

† Present address: Department of Physics, Faculty of Science, University of Tokyo, Bunkyo-ku, Tokyo 113.

© Astronomical Society of Japan • Provided by the NASA Astrophysics Data System

1986PASJ...38..731S

1. Introduction

Vela X-1 (4U 0900−403) is known as an eclipsing X-ray binary with an orbital period of 8.96 d (Forman et al. 1973) and a pulsation period of 283 s (McClintock et al. 1976; Rappaport et al. 1976). The eclipse ephemerides, the pulse-period changes, and the orbital elements of this X-ray pulsar have been continually studied over ten years (Rappaport et al. 1980; Nagase et al. 1983, 1984a; van der Klis and Bonnet-Bidaud 1984; Boynton et al. 1984, 1986, and references therein). The companion star HD 77581 was found by optical and ultraviolet observations to be an early-type supergiant (B0.5 Ib) at a distance of 1.9 kpc emanating an intense stellar wind (van Paradijs et al. 1977; Dupree et al. 1980; van Genderen 1981; Sadakane et al. 1985, and references therein). The stellar and binary parameters of the Vela X-1/HD 77581 system, summarized previously by Conti (1978), are updated in table 1 of Nagase et al. (1986, hereafter referred to as paper I).

The eclipse duration of Vela X-1 was determined to be 1.7 d (Watson and Griffiths 1977; Nagase et al. 1983; van der Klis and Bonnet-Bidaud 1984, and references therein). This gives a lower limit of 74° for the inclination angle of the binary system by considering other stellar and binary parameters (Joss and Rappaport 1984). An orbital phase dependence of X-ray absorption was observed by the Hakucho satellite and was explained in term of a nonuniform gas distribution by Nagase et al. (1983). An asymmetric decrease of the X-ray intensity at ingress and egress of Vela X-1 was observed with the Ariel V satellite (Watson and Griffiths 1977) and the Hakucho satellite (Nagase et al. 1983). Becker et al. (1978) detected a residual X-ray flux during the eclipse, at a level of about 2% of the uneclipsed flux.

An emission line feature at $\sim$6.8 keV was found by Becker et al. (1978), whereas White et al. (1983) reported the line energy observed by the HEAO-1 experiment to be consistent with 6.4 keV. Ohashi et al. (1984) determined the iron line energy more precisely to be 6.43 ± 0.05 keV by the Tenma observations. They also found the iron line emission during the eclipse period of Vela X-1 but did not find any evidence for the pulsation of the iron line, thus indicating an extended reprocessing site for fluorescent line emission. Further results on the X-ray spectra, obtained with Tenma during noneclipse periods in March 1983, were described in paper I.

The variations of the continuum X-ray flux and the iron line intensity throughout the eclipse provide a useful probe to investigate the distribution of matter surrounding the Vela X-1/HD 77581 binary system, the mass accretion by the neutron star from the stellar wind of the companion star, and the structure of the atmosphere thereof. The companion star plays the role of an occulter in investigations near the neutron star. For this purpose, we observed Vela X-1 throughout an eclipse in March 1984. The orbital phase dependences of the iron line intensity and the absorption column density are derived by including the results of March 1983 as well, paying special attention to those in the phase near the eclipse. We discuss the stellar atmosphere extending over the companion star and the reprocessing sites of the fluorescence iron line, the detailed properties of which are obtained owing to the superior energy resolution of the gas scintillation counters (GSPCs) aboard the Tenma satellite.

© Astronomical Society of Japan • Provided by the NASA Astrophysics Data System

1986PASJ...38..731S

2. Observations and Results

The observations of Vela X-1 were performed with the GSPCs aboard Tenma on March 22 through 27, 1984, covering an interval of about half the orbital period and one complete eclipse event. In our analysis we used the data observed with four counters in the SPC-A system with a field of view of 3°.1 FWHM and three counters in the SPC-B system with a field of view of 2°.5 FWHM, the total effective area being 560 cm^2 (Tanaka et al. 1984) with an energy resolution of $\sim 10\%$ at 6–7 keV (Koyama et al. 1984). Data from one counter (SPC-B No. 6) were discarded because of the degraded energy resolution. Background data were taken from a source-free sky region near Vela X-1. We carefully avoided the confusion with nearby weak X-ray sources. Especially, for the analysis throughout the eclipse phase, we discarded the data which include at least one of the X-ray sources, 1H 0900−374 [0.8 UFU (Uhuru flux unit)], 1H 0908−326 (1.2 UFU) and 1H 0910−374 (0.8 UFU), in the field of view of the GSPCs within 2°.5, and 1H 0850−42 (0.55 UFU) within 2°.0 from the optical axis. We confirmed that the source contamination is at most 20% and 15%, respectively in the range 2–6 keV and 6–10 keV for the energy spectrum during the eclipse phase.

2.1. *Pulse Period*

The pulse period was obtained from the timing analysis of heliocentric pulse arrival times measured during the noneclipse phase. Since the time span of the present observations is rather limited, we fixed the orbital parameters to the values determined from our previous observations (Nagase et al. 1984b), and obtained the pulse period of $P_0 = 282.912 \pm 0.005$ s. Because of the short time span of the data set, we were unable to obtain a finite value of $\dot{P}$ during the observations. The tendency of a constant pulse period (Nagase et al. 1984a) has continued over two years, although a slight spin-up of $\dot{P}/P_0 \simeq -2 \times 10^{-5}\ yr^{-1}$ is suspected during the two years between 1982 and 1984.

2.2. *X-Ray Light Curve*

The X-ray light curves in three energy ranges, 2–6 keV, 6–10 keV, and 10–20 keV are shown in figure 1 after subtracting the background and correcting for the satellite aspect. Each point in this figure shows the average flux accumulated for a net time span of 400–1500 s. A sharp decrease in the X-ray flux, with a transit time of ~ 5 hr, is seen during each of the eclipse immersion and emersion. During the eclipse period, we observed finite fluxes of $(1.21 \pm 0.08) \times 10^{-3}$ counts $cm^{-2}\ s^{-1}$ in 2–6 keV, $(1.31 \pm 0.08) \times 10^{-3}$ counts $cm^{-2}\ s^{-1}$ in 6–10 keV, and $(0.82 \pm 0.11) \times 10^{-3}$ counts $cm^{-2}\ s^{-1}$ in 10–20 keV, respectively, corresponding to 3.2%, 2.0%, and 0.9% of the respective noneclipse fluxes.

The entry or exit time (phase) of the X-ray source is defined here as the point where an exponential fit to the decreasing intensity crosses the average eclipse flux. The mid-eclipse time T_{mid}, the eclipse duration ΔT_{ecl}, and the transit times at immersion ΔT_{in} and at emersion ΔT_{out} are shown in figure 1, and their values thus determined are listed in table 1 for the three energy ranges. We obtained the duration of $\Delta T_{ecl} = 1.72 \pm 0.04$ d and the mid-eclipse time of $T_{mid} =$ JD 2,445,785.22 $\pm$ 0.04, respectively

© Astronomical Society of Japan • Provided by the NASA Astrophysics Data System

1986PASJ...38..731S

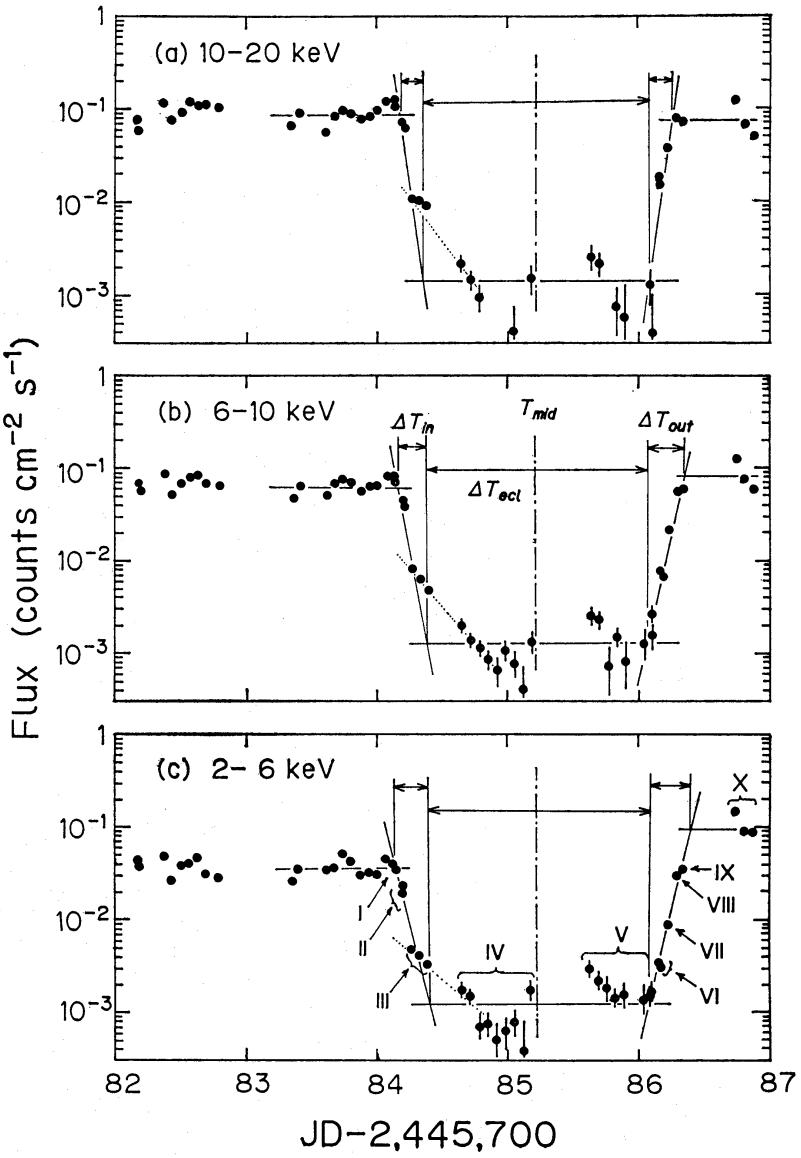

Fig. 1. The X-ray light curve of Vela X-1 in the three energy bands (a) 10–20 keV, (b) 6–10 keV, and (c) 2–6 keV, observed with the GSPC system (560 cm^2 of effective area) aboard Tenma on March, 1984, covering an eclipsing phase. Each point usually corresponds to a net integration time of 400–1500 s. The mid-eclipse time $T_{\rm mid}$, the transit times at immersion $\Delta T_{\rm in}$ and at emersion $\Delta T_{\rm out}$, and the duration of eclipse $\Delta T_{\rm ecl}$ are indicated in the figure for each energy band. The values of these parameters are listed in table 1. The solid lines represent the light curves expected from the absorption by the companion stellar atmosphere and those expected from the residuals scattered by the stellar wind during the eclipse, while the dotted lines simulate the contribution of X-rays scattered by a wake behind the neutron star. Phases I–X indicated in (c) are referred to throughout the present paper.

averaged over the three energy ranges. The duration derived is consistent with the previous reports (Watson and Griffiths 1977; Nagase et al. 1983).

The observed transit times at immersion and emersion are in fact shorter in the higher energy range as is expected from the absorption by the stellar atmosphere discussed later. The observed decrease of flux at immersion is relatively steep in

© Astronomical Society of Japan • Provided by the NASA Astrophysics Data System

1986PASJ...38..731S

Table 1. Epoch and duration of Vela X-1 eclipse observed with Tenma in March 1984.

Quantity	Energy band		
	2–6 keV	6–10 keV	10–20 keV
Transit time at entry: $\Delta T_{\rm in}$ (hr)	5.1 ±0.7	4.4 ±0.8	3.8 ±0.7
Transit time at exit: $\Delta T_{\rm out}$ (hr)	5.9 ±0.8	5.4 ±0.7	4.5 ±0.8
Eclipse duration: $\Delta T_{\rm ecl}$ (d)	1.74±0.06	1.71±0.06	1.71±0.05
Eclipse half angle: $\Theta_{\rm ecl}$ (degree)	35.0 ±1.3	34.4 ±1.3	34.4 ±1.1
Mid-eclipse time: $T_{\rm mid}$ (JD−2,445,700)	85.23±0.06	85.22±0.06	85.22±0.06

contrast with that in the previous observations. The X-ray data observed by COS-B (van der Klis and Bonnet-Bidaud 1984) indicated that the transit time at ingress changed from orbit to orbit. A gradual decrease in intensity, shortly after ingress, is noticed in all the three energy ranges as shown by dotted lines in figure 1, which will be attributed to the accretion wake as discussed later. Contrary to the transit at ingress, all observations at egress give a consistent transit time of $\sim$5 hr, or $\Delta\Phi_{\rm out}\simeq 0.023$ (Watson and Griffiths 1977; Nagase et al. 1983; van der Klis and Bonnet-Bidaud 1984).

The time of superior conjunction of the X-ray source is estimated to be $T_{\rm conj}=$ JD 2,445,785.28±0.08 from the periastron passage time T_ω determined by the timing analysis. This value of $T_{\rm conj}$ is consistent with the mid-eclipse time $T_{\rm mid}$ obtained above within the accuracy of determination, as it is larger than the expected difference of $T_{\rm mid}-T_{\rm conj}=20$ min (van der Klis and Bonnet-Bidaud 1984). We obtain the orbital period of $P_{\rm orb}=8.96426\pm0.00018$ d together with an insignificant time derivative of $(\dot{P}/P)_{\rm orb}=(0.9\pm1.4)\times10^{-5}$ yr^{-1} during the interval 1975–1984, combining our observation of the eclipse center, $T_{\rm mid}$, with the previous ones [table 4 in van der Klis and Bonnet-Bidaud (1984)]. This value is consistent with that derived from the timing analysis of pulse arrival times (Nagase et al. 1984b; Boynton et al. 1986).

2.3. *Pulse Profile*

Vela X-1 is known by its complex pulse profiles, i.e., the saw-toothlike double peak in the higher energy range and the spiky five peaks in the lower energy range (McClintock et al. 1976; Bautz et al. 1983; Nagase et al. 1983; White et al. 1983). In figure 2, we show the normalized pulse profiles in three energy ranges along the course of emersion of the X-ray source from eclipse. In each profile, several successive pulses observed in a satellite orbit are superposed modulo the best-fit apparent pulse period at the corresponding orbital phase. The pulse amplitudes are normalized by the pulse averaged flux after subtracting the background, so as to directly compare the amplitudes with each other. Observation times and orbital phases of the pulse profiles shown in figure 2 are given in table 2 together with the average flux and the relative amplitude of modulation normalized by the master template of the pulse profile observed at $\Phi_{\rm orb}=0.17$–0.19 (data number X in figure 1). We can hardly find the pulse modulation in any of the three energy ranges of the residual flux during eclipse as demonstrated in the upper panels of figure 2. One can see that the normalized pulse

© Astronomical Society of Japan • Provided by the NASA Astrophysics Data System

1986PASJ...38..731S

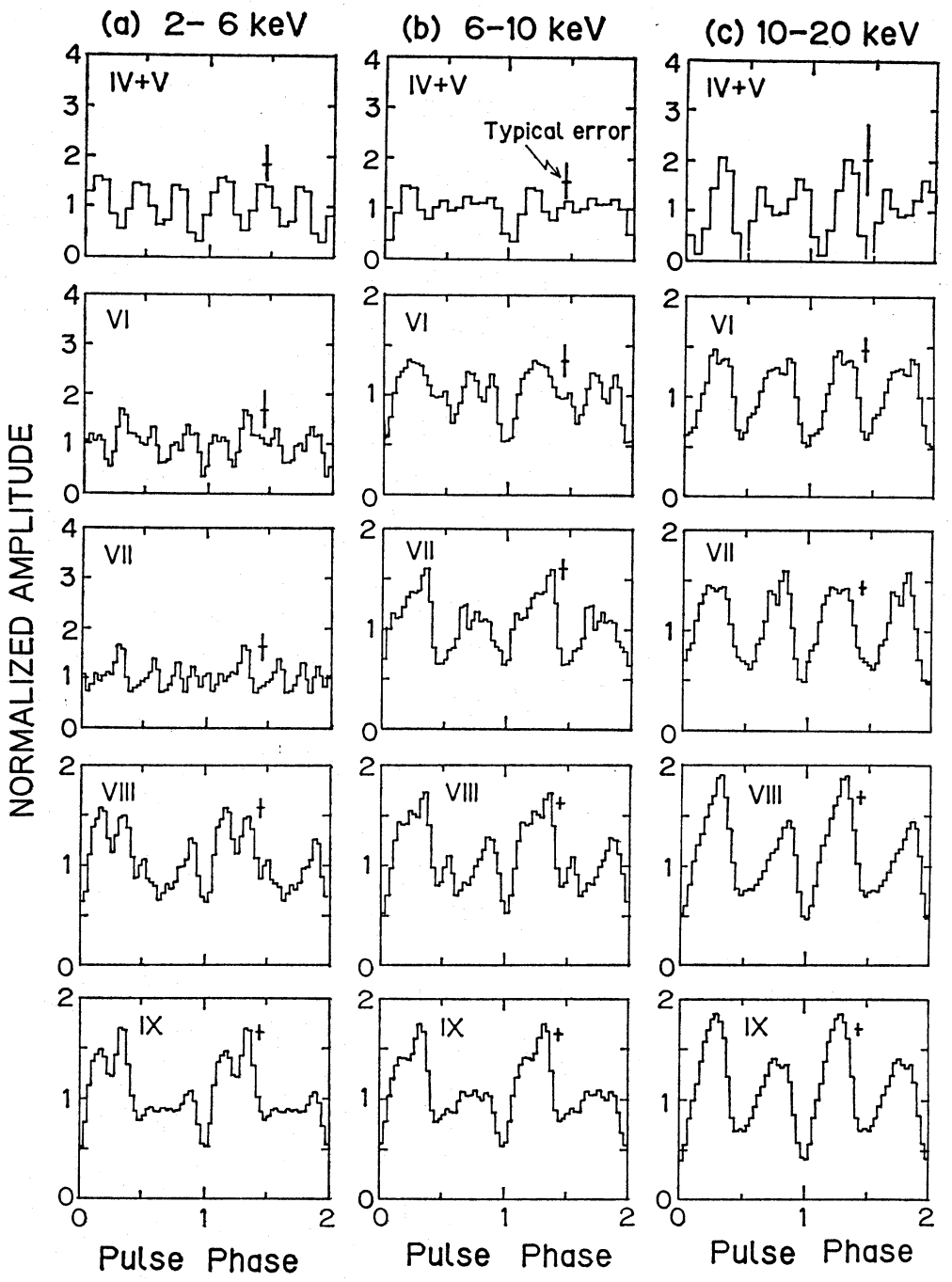

Fig. 2. The evolution of the pulse profiles along the course of emersion of Vela X-1 from eclipse (data IV through IX of figure 1) for energy ranges (a) 2–6 keV, (b) 6–10 keV, and (c) 10–20 keV. The data are smoothed by taking the running average of adjacent bins to improve statistics. The pulse profiles are normalized by the pulse averaged flux so as to give the normalized pulse amplitude. Note that the pulse profiles are composed of the data only from SPC-A system (320 cm^2).

amplitude increases with the orbital phase in the increasing order of energy. It is interesting that the pulse amplitudes at phases VI and VII during emersion are considerably suppressed, compared with those during the noneclipse phase (data X) in all

© Astronomical Society of Japan • Provided by the NASA Astrophysics Data System

1986PASJ...38..731S

Table 2. Evolution of pulse profiles along the emersion of Vela X-1 observed from Tenma in March 1984.

Physical quantity	Phase					
	IV+V	VI	VII	VIII	IX	X (master)
Observation date and time	25 March 3: 33–26 March 14: 29	26 March 15: 53	26 March 27: 27	26 March 19: 02	26 March 20: 07	27 March 5: 45–9: 13
Orbital phase	0.936–0.099 (eclipse)	0.106	0.114	0.121	0.127	0.170–0.186
			2–6 keV			
Flux, f_{av}[a]	1.18±0.11	3.47±0.32	8.07±0.35	29.10±0.40	33.85±0.37	100.99±0.51
Amplitude, A_{rel}[b]	−0.04±0.44[c]	0.48±0.31	0.27±0.15	0.97±0.06	1.01±0.04	1.00[b]
			6–10 keV			
Flux, f_{av}[a]	1.24±0.10	7.72±0.32	21.09±0.37	52.73±0.51	57.54±0.44	81.18±0.47
Amplitude, A_{rel}[b]	0.05±0.39[c]	0.52±0.13	0.78±0.06	0.91±0.03	0.98±0.03	1.00[b]
			10–20 keV			
Flux, f_{av}[a]	0.64±0.15	17.34±0.47	35.37±0.40	70.16±0.63	66.78±0.53	72.47±0.53
Amplitude, A_{rel}[b]	0.37±1.04[c]	0.77±0.08	0.86±0.04	1.00±0.03	1.10±0.03	1.00[b]

[a] f_{av}; pulse averaged fluxes in units of 10^{-3} counts cm^{-2} s^{-1}.

[b] A_{rel}; relative pulse amplitudes in reference to the "master" pulses, which consist of those observed during the noneclipse phase at Φ_{orb}=0.170–0.186.

[c] Pulse profiles during the eclipse consist of data in 16 bins of the pulse phase, while others consist of data in 32 bins (see figure 2).

© Astronomical Society of Japan • Provided by the NASA Astrophysics Data System

1986PASJ...38..731S

the three energy ranges, although the pulse amplitude also fluctuates considerably even during the noneclipse phase. Whereas, the relative amplitudes at VIII and IX are almost comparable with those at the noneclipse phase (X) in all the three energy ranges in spite of the clear evidence of low-energy absorption as indicated in table 2. These features can be interpreted in terms of absorption and/or scattering by matter in the extended atmosphere of the companion star. Details will be discussed in the next section.

2.4. *Energy Spectra*

All the pulse height spectra obtained in the present observations are analyzed in the same manner as the fitting procedure described in paper I. In figure 3a, the observed spectra are shown in the course of the X-ray source immersion to the eclipse; i.e., (I) at $\Phi_{\rm orb}=0.881$, just before the ingress, (II) at $\Phi_{\rm orb}=0.888$, and (III) at $\Phi_{\rm orb}=0.895$–0.908, both during immersion, and (IV) at $\Phi_{\rm orb}=0.938$–0.997, in the first half of the eclipse. In figure 3b, those in the course of emersion from the eclipse are

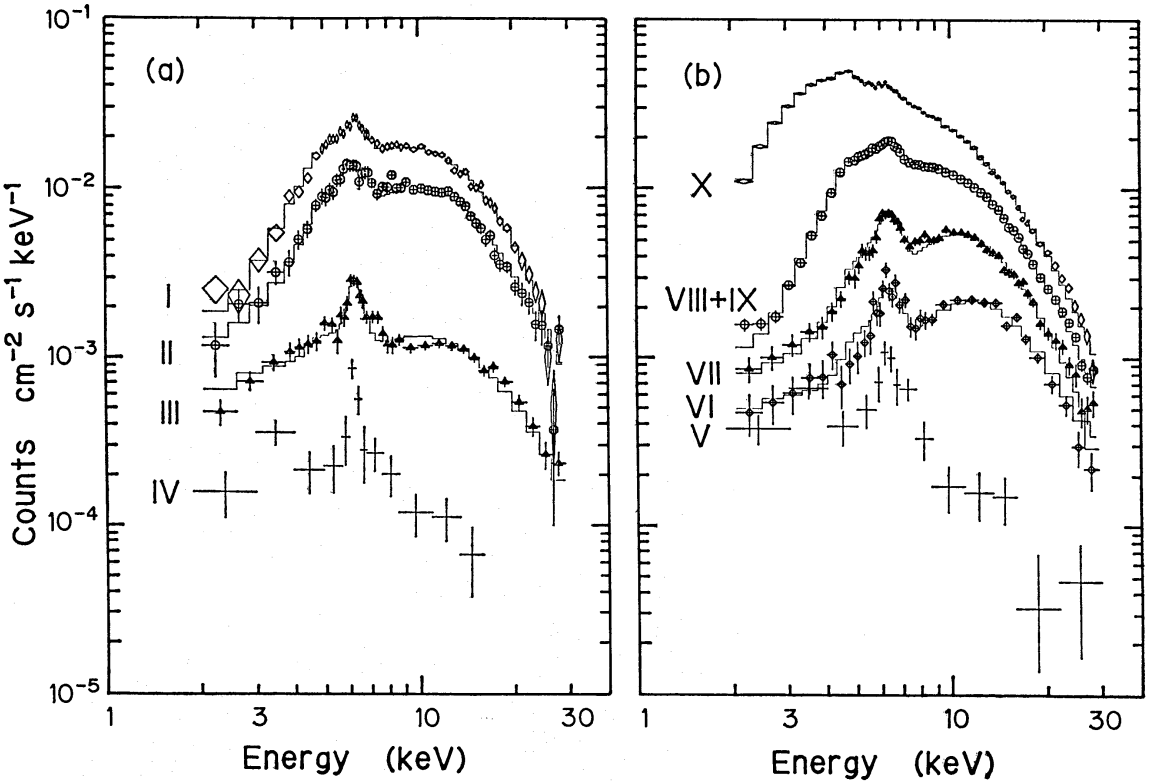

Fig. 3. The pulse-averaged energy spectra of Vela X-1 observed with Tenma throughout the eclipse. (a); the change of spectra in the course of immersion of Vela X-1 observed at (I) $\Phi_{\rm orb}=0.881$, (II) $\Phi_{\rm orb}=0.888$, (III) $\Phi_{\rm orb}=0.895$–0.908, and (IV) $\Phi_{\rm orb}=0.938$–0.997, respectively. (b); those in the course of emersion of Vela X-1 observed at (V) $\Phi_{\rm orb}=0.049$–0.099, (VI) $\Phi_{\rm orb}=0.106$, (VII) $\Phi_{\rm orb}=0.114$, (VIII) $\Phi_{\rm orb}=0.121$, (IX) $\Phi_{\rm orb}=0.127$, and (X) $\Phi_{\rm orb}=0.179$, respectively corresponding to the data points indicated at the bottom panel of figure 1. The solid lines represent the best-fit model spectra with a power-law continuum, an iron fluorescence line, and circum/interstellar absorption. A clumped blob model was adopted in the fitting for the low-energy absorption, though data I, II, VIII, IX, and X are consistent with homogeneous absorption.

© Astronomical Society of Japan • Provided by the NASA Astrophysics Data System

1986PASJ...38..731S

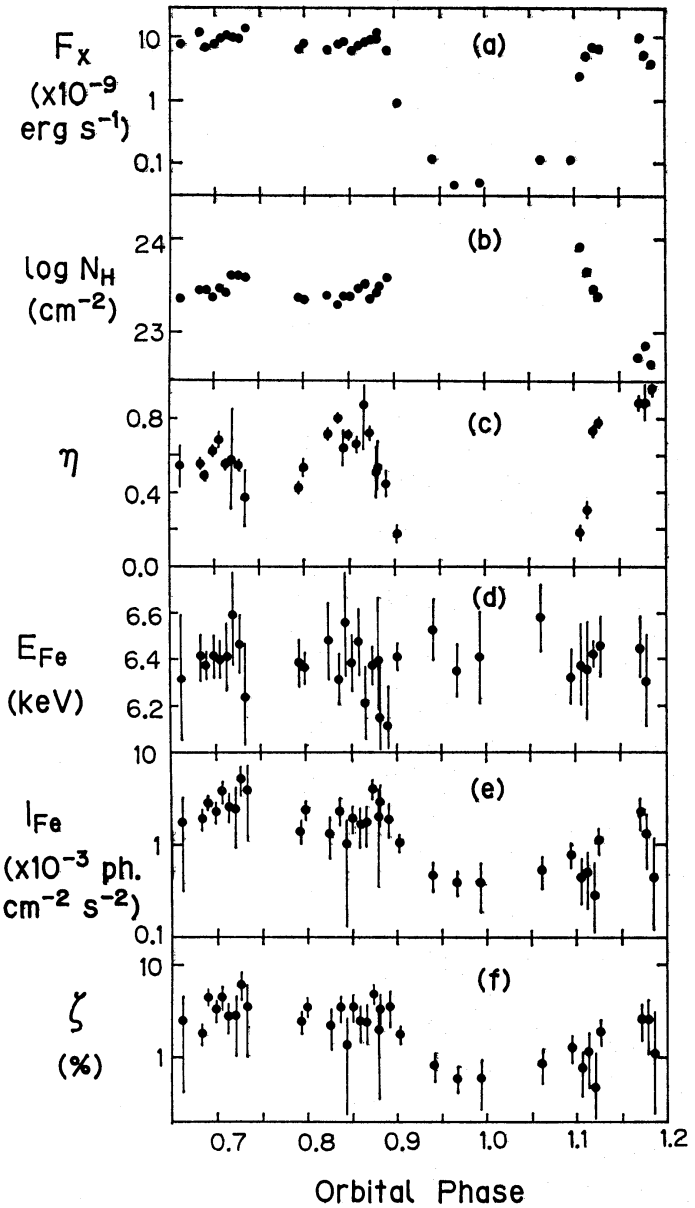

Fig. 4. The best-fit spectral parameters as functions of orbital phase: (a) energy flux, F_X, in the range 2–30 keV in units of 10^{-9} erg cm^{-2} s^{-1}, (b) absorption column density, log N_H, where N_H is given in units of H-atoms cm^{-2}, (c) reduction factor, η, of optical depth (see text), (d) energy, E_{Fe}, of the fluorescence Kα line of iron in keV, (e) intensity, I_{Fe}, of the iron line in units of 10^{-3} photons cm^{-2} s^{-1}, and (f) relative line intensity, ζ (see text). All quoted errors represent 90% confidence limits for a single parameter.

shown; i.e., (V) at Φ_{orb}=0.049–0.099, in the second half of the eclipse, (VI) at Φ_{orb}=0.106, (VII) at Φ_{orb}=0.114 and the sum of (VIII) at Φ_{orb}=0.121 and (IX) at Φ_{orb}=0.127, all the three during emersion, and (X) at Φ_{orb}=0.179, just after the egress. The iron line emission feature becomes conspicuous, as the orbital phase Φ_{orb} approaches the eclipse, thus indicating that the fluorescence emission of the iron line is relatively effective compared with scattering of continuum.

© Astronomical Society of Japan • Provided by the NASA Astrophysics Data System

1986PASJ...38..731S

Spectra of Vela X-1 during the noneclipse phase can be well fitted to a power law spectrum with a high-energy cutoff and a low-energy absorption, on which a narrow emission line is superposed as was discussed in paper I. The photoelectric absorption cross section for interstellar matter is adopted from Morrison and McCammon (1983) to determine the column density for the low-energy absorption, but the iron abundance is changed to $N_{\rm Fe}=3.8\times10^{-5}\,N_{\rm H}$ according to paper I. Although the scattering cross section is not included in the present analysis, the contribution of scattering is irrelevant to the derivation of $N_{\rm H}$, because the cross section is essentially energy independent.

The parameters characterizing each spectrum are plotted as functions of orbital phase in figure 4. All the quoted errors in the figure represent 90% confidence limits for each parameter. These are (a) the energy flux $F_{\rm X}$ in the range 2–30 keV, (b) the absorption column density $N_{\rm H}$, (c) the reduction factor, η, of optical depth at 3 keV, (d) the energy of the fluorescence iron line $E_{\rm Fe}$, (e) the line intensity $I_{\rm Fe}$, and (f) the relative line intensity ζ. The reduction factor, η, of the optical depth due to the inhomogeneity of the absorbing matter is simulated by the clumped blob model (paper I) and defined by

$$\eta\equiv\frac{\tau_{\rm eff}}{\tau}=\frac{1-\exp\left(-\tau_{\rm b}\right)}{\tau}\,, \tag{1}$$

where $\tau_{\rm eff}=\nu_0[1-\exp\left(-\tau_{\rm b}\right)]$ is an effective optical depth for the clumped matter. $\tau\,(=N_{\rm H}\sigma_0)$ is an optical depth expected for the homogeneous cool matter with a column density $N_{\rm H}$ and a photoelectric cross section σ_0. Here $N_{\rm b}$, ν_0, and $\tau_{\rm b}(=\sigma_0 N_{\rm b})$ are the column density of a blob, the average number of blobs along the line of sight, and the optical depth of a blob, respectively. The relative line intensity ζ is defined by

$$\zeta\equiv I_{\rm Fe}\Big/\int_{E_{\rm K}}^{\infty} f(E)\frac{\sigma_{\rm Fe}(E)}{\sigma_{\rm Fe}(E_{\rm K})}\,dE \tag{2}$$

to estimate the effective fluorescence efficiency, where $f(E)$, $E_{\rm K}$, and $\sigma_{\rm Fe}(E)$ are the incident photon spectrum, the iron K-edge energy, and the photoabsorption cross section of iron, respectively. These values during the noneclipse phase are consistent with those observed in March 1983 (Ohashi et al. 1984; paper I), whereas those near and during the eclipse are new information acquired in the present observations. The average of the iron Kα-line energies in figure 4d gives a value of 6.43 ± 0.05 keV, consistent with that obtained by Ohashi et al. (1984) and in paper I for the March 1983 observations. We note that emission line during eclipse was also observed at 6.4 keV, thus indicating the fluorescent emission reprocessed by an extended region of cool matter. The energy of the iron K-absorption edge is determined to be 7.25 ± 0.05 keV from the spectra observed between $\Phi_{\rm orb}=0.65$ and 0.88 and is also consistent with that obtained in paper I.

The soft-excess feature, i.e., an excess of the X-ray flux in the low-energy range (2–4 keV) over that expected for the absorption by the cool homogeneous matter, is remarkable in the spectra observed during the orbital phase $\Phi_{\rm orb}=0.65$–0.80, thus, yielding a small value of η as seen in figure 4c. The features of such a soft excess ob-

© Astronomical Society of Japan • Provided by the NASA Astrophysics Data System

1986PASJ...38..731S

served would look similar to the phenomena observed occasionally during the non-eclipse phase in March 1983 (paper I). The best-fit convolved spectra by a clumped blob model are shown by solid lines on respective spectra of figure 3 except for those observed during the eclipse phases (IV) and (V), details of which will be discussed in section 3.3. However, the simple clumped-blob model described above can hardly fit the spectrum III as seen in figure 3. Though the fitting by the clumped blob model was performed throughout immersion and emersion, it should be noted that the small η-values obtained from the data during immersion and emersion at phases (III), (VI), and (VII) are artifacts, and indicate a superposition of the scattered soft X-rays and the highly absorbed hard X-rays coming directly from the source, as discussed in section 3.1.

The average iron line intensity during the eclipse is $(5.1\pm1.2)\times10^{-4}$ photons cm^{-2} s^{-1}, corresponding to $15.0\pm5.4\%$ of that in the noneclipsing phase, in contrast to a decrease of the continuum flux by two orders of magnitude. This iron line intensity during the eclipse observed in March 1984 is about twice as large as that of $(2\pm1)\times10^{-4}$ photons cm^{-2} s^{-1} observed in March 1983 by Ohashi et al. (1984).

3. Discussion

3.1. *Extended Atmosphere of the Companion Star*

As mentioned in the previous section, the X-ray light curves of Vela X-1 during

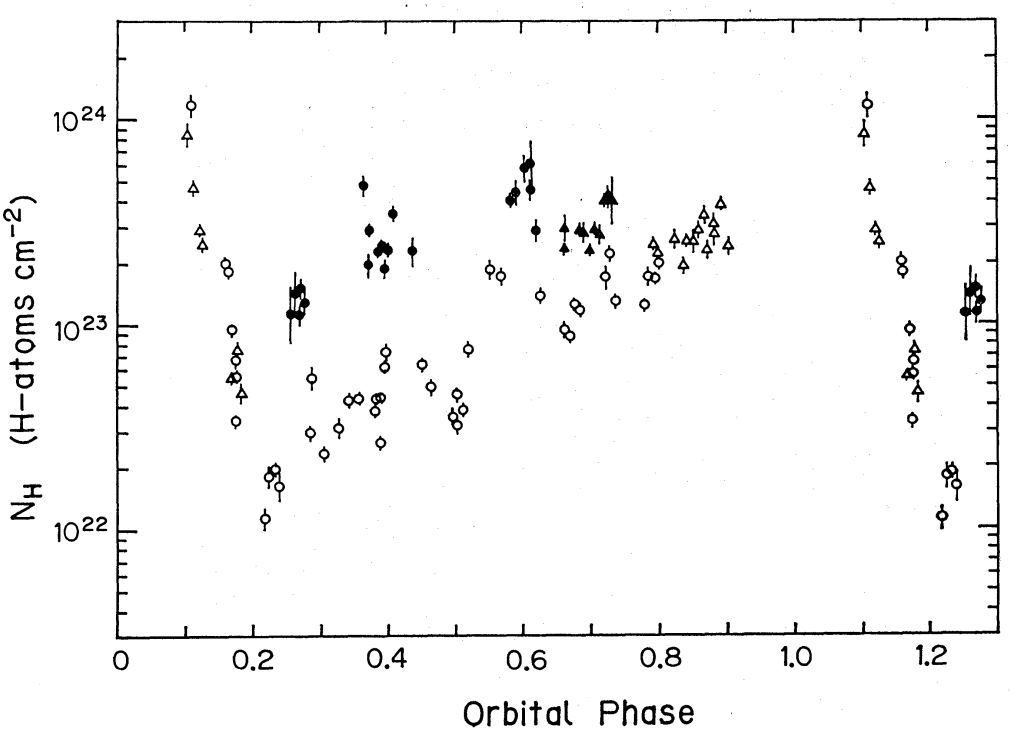

Fig. 5. The absorption column density N_H as a function of the orbital phase. Filled and open circles represent the data obtained in March 1983, whereas filled and open triangles are the data obtained in March 1984. Filled circles and triangles indicate the data obtained for the spectra with soft-excess feature ($\eta\lesssim0.7$) caused by the inhomogeneous absorption.

© Astronomical Society of Japan • Provided by the NASA Astrophysics Data System

1986PASJ...38..731S

the egress have a common feature with a transit time of ~ 5 hr, whereas the light curves during the ingress show different features in different observations (Watson and Griffiths 1977; Nagase et al. 1983; van der Klis and Bonnet-Bidaud 1984). The absorption column density measured with Tenma is shown in figure 5 as a function of the orbital phase. The circles and the triangles in the figure indicate the absorption measures observed in March 1983 and those in March 1984, respectively, where those with filled symbols are derived from spectra with a soft excess feature.

The global feature of the X-ray absorption is characterized by a steep exponential decrease from $N_{\rm H}\simeq 1\times 10^{24}$ H-atoms cm^{-2} at $\Phi_{\rm orb}\simeq 0.1$ (just after egress) to $N_{\rm H}\simeq 2\times 10^{22}$ cm^{-2} at $\Phi_{\rm orb}\simeq 0.2$ and a gradual increase to $N_{\rm H}\simeq 3\times 10^{23}$ cm^{-2} thereafter to $\Phi_{\rm orb}=0.9$ (just before ingress). The gradual increase of the absorption measure in proportion to the orbital phase suggests a stationary condensation of matter in the accretion wake behind the neutron star. The lowest value of $N_{\rm H}\simeq 2\times 10^{22}$ cm^{-2} observed at $\Phi_{\rm orb}\simeq 0.25$, on the contrary, may be attributed to a stationary stellar wind. The exponential increase of the absorption measure up to $N_{\rm H}\simeq 1\times 10^{24}$ cm^{-2} toward the decreasing orbital phase to $\Phi_{\rm orb}\simeq 0.1$ is considered to arise from the extended atmosphere of the companion star.

The extended atmosphere is modeled by a combination of a spherical atmosphere of scale height H and a spherical stellar wind. Hence the density of matter at a radial distance, r, from the center of the companion star can be expressed as

$$\rho(r)=\rho_0 \exp\left(-\frac{r-R_*}{H}\right)+\frac{\dot{M}_*}{4\pi r^2 v_{\rm w}(r)}, \tag{3}$$

where R_* is the radius of the companion star, M_* the mass-loss rate in the wind of the companion star, and $v_{\rm w}$ the wind velocity. The scale height is given by a hydrostatic model as

$$H=\frac{kT_{\rm eff}}{\mu m_{\rm H} g_{\rm eff}}, \quad g_{\rm eff}=g\left(1-\frac{\kappa L_*}{4\pi cGM_*}\right), \tag{4}$$

where $T_{\rm eff}$ is the effective temperature, $g_{\rm eff}$ the effective gravity, L_* and M_* the luminosity and the mass of the companion star, $m_{\rm H}$ the hydrogen mass, and μ the mean molecular weight. The mass-loss rate of HD 77581 has been estimated to be $\dot{M}_*=1\times 10^{-6}$ $M_\odot$ yr^{-1} by Dupree et al. (1980) and $\dot{M}_*=4\times 10^{-6}$ $M_\odot$ yr^{-1} by McCray et al. (1984). Optical studies of early-type giants/supergiants give the radial dependence of the wind velocity in the form

$$v_{\rm w}(r)=v_0+v_\infty(1-R_*/r)^\beta, \tag{5}$$

where v_∞ is the terminal velocity, which generalizes the theory of Castor et al. (1975) with the velocity law of $\beta=1/2$. Using equation (3), we have calculated the orbital phase dependence of column density assuming the following wind parameters based on the observations by Dupree et al. (1980); i.e., $v_0=30$ km s^{-1}, $v_\infty=1600$ km s^{-1}, and $\beta=1/2$. This set of parameters gives a wind velocity of $v_{\rm w}$ ($r=1.7R_*$)$\simeq 1000$ km s^{-1} at the orbit of the neutron star. The scale height of $H=(2.7\pm 0.8)\times 10^{11}$ cm [$=(0.14\pm 0.04)R_*$], the density at the base of the atmosphere of $\rho_0=(5.7\pm 0.5)\times 10^{-12}$ g cm^{-3},

© Astronomical Society of Japan • Provided by the NASA Astrophysics Data System

1986PASJ...38..731S

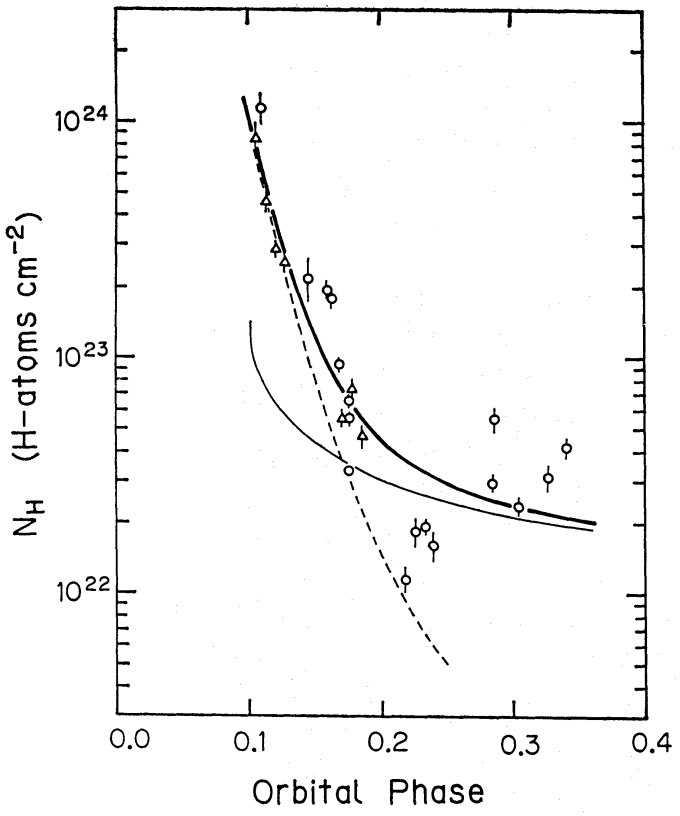

Fig. 6. The absorption column density at the orbital phase Φ=0.1–0.35, excluding the data associated with the soft-excess feature (filled circles in figure 5). The thick solid curve indicates the column density calculated from the sum of the stellar atmosphere (dashed curve) and the stellar wind (thin solid curve).

and the mass-loss rate of $\dot{M}_*=(2.4\pm1.2)\times10^{-6}\ M_\odot\ \mathrm{yr}^{-1}$ are required to explain the change of the measured column density between orbital phases 0.3 and 0.1. The data derived from the soft-excess spectra (filled symbols in figure 5) are excluded to obtain the parameters, and the errors in the above values are determined by taking into account the scattering of the data points. The orbital phase dependence of the absorption measure expected from equation (3) using these values is compared with the observed absorption measure in figure 6, in which the portion of Φ_{orb}=0.1–0.35 is enlarged. The effect of absorption by the atmosphere revealed by the intensity decrease near the eclipse shown in figure 1 and table 1 is thus explained by the above model of the atmosphere.

On the other hand, the scale height of the hydrostatic atmosphere is estimated to be $H\simeq1\times10^{10}$ cm for $T_{\mathrm{eff}}\simeq26{,}000$ K (Sadakane et al. 1985) and $g_{\mathrm{eff}}\simeq0.5\ g$ with the Thomson scattering opacity $\kappa_{\mathrm{Th}}=0.34\ \mathrm{cm}^2\ \mathrm{g}^{-1}$, $\mu=0.6$, $L_*=1.3\times10^{39}\ \mathrm{erg\ s}^{-1}$, and $M_*=23\ M_\odot$. This value of H is smaller than that deduced here by a factor of 30. Hence our observation indicates that the stellar atmosphere of the early-type supergiant star HD 77581 is more extended. The scale height of 3×10^{11} cm indicates $\kappa/\kappa_{\mathrm{Th}}\simeq2$. Since the atmospheric gas contains partially ionized heavy elements, their resonance lines contribute to the opacity κ to increase the scale height. In fact, our result of $H\simeq0.14R_*$ is consistent with an estimate for a line driven wind by Friend and Castor (1982). Clark and Minato (1985) also found a large scale height of $H\simeq7.5\times$

© Astronomical Society of Japan • Provided by the NASA Astrophysics Data System

1986PASJ...38..731S

10^{10} cm ($\simeq 0.1 R_*$) for the companion star (O 6.5 giant, Krzemiński's star) of Cen X-3.

The evolution of the pulse profile during the emersion of Vela X-1 exhibits evidence for X-ray scattering by the extended stellar atmosphere. Pulse profiles observed during eclipse (IV+V of figure 2) do not show any evidence of pulse modulation, indicating that the whole residual flux is of the scattering origin. Interesting features can be seen in the pulse profiles in phases VI and VII of figure 2, which were observed around $\Phi_{\rm orb} \simeq 0.11$ when the line of sight crossed the stellar atmosphere. The relative pulse amplitudes of these profiles are significantly diminished in all the three energy bands compared with those during the noneclipse phase. There is no evidence of the pulse-phase shift and the smearing effect of the pulse shape is not conspicuous in phases VI and VII.

The above features can be explained in terms of scattering as follows. As the X-rays passing through the stellar atmosphere meet with dense matter of the column density of $N_{\rm H} \simeq 10^{24}$ cm^{-2}, for which the optical depth for scattering is nearly unity, more than a half of the X-rays emanated from the neutron star lose the memory of the pulse shape due to scattering, since the time delay by scattering is several tens of second. Hence the pulse amplitude of incoming X-rays would be degraded by a factor of two or so. It is noted that scattering does not strongly change the pulse shape, if the original pulse has a broad sinusoidal shape, like the one observed from Vela X-1 in its high energy range. The effect of scattering is nearly independent of X-ray energy in the energy range concerned, thus resulting in the energy independent modulation of the normalized amplitude.

The effect of scattering is also seen from the light curve which shows a gradual decrease during immersion after the steep decrease due to the atmospheric absorption, as shown by the dotted lines in figure 1. The X-ray intensity at this phase is about one tenth of that at the noneclipse phase in all the energy ranges. The fact that the gradual decrease was conspicuous during immersion but not during emersion suggests the contribution of the accretion wake behind the neutron star to the scattering. Spectrum III observed at this phase is explained by the superposition of the spectrum absorbed and scattered by the dense wake and/or the atmosphere and that scattered by the stationary stellar wind with a relatively low column density.

3.2. *Iron Line Emission from the Stellar Wind*

The intensity of the iron emission line of $\sim 5 \times 10^{-4}$ photons cm^{-2} s^{-1} during the eclipse provides firm evidence for the contribution of the stellar wind to the iron iron fluorescence. The iron line intensity in figure 7a indicates a broad orbital phase dependence, and its value during the eclipse is about 15% of that during the nonclipse phase.

Since the intensity the fluorescence iron line depends on the X-ray luminosity and the spectrum emitted from the X-ray source, we show in figure 7b the relative line intensity ζ, normalized to the emitted continuum by equation (2), as a function of the orbital phase. For the eclipse phase we assume that the emitted continuum is the same as the average over the noneclipse phase. The relative line intensity thus derived is on the average $\sim 0.7\%$ for the eclipse phase, while it ranges between 2–8% otherwise. Also figure 7b shows the orbital phase dependence more clearly than the raw

© Astronomical Society of Japan • Provided by the NASA Astrophysics Data System

1986PASJ...38..731S

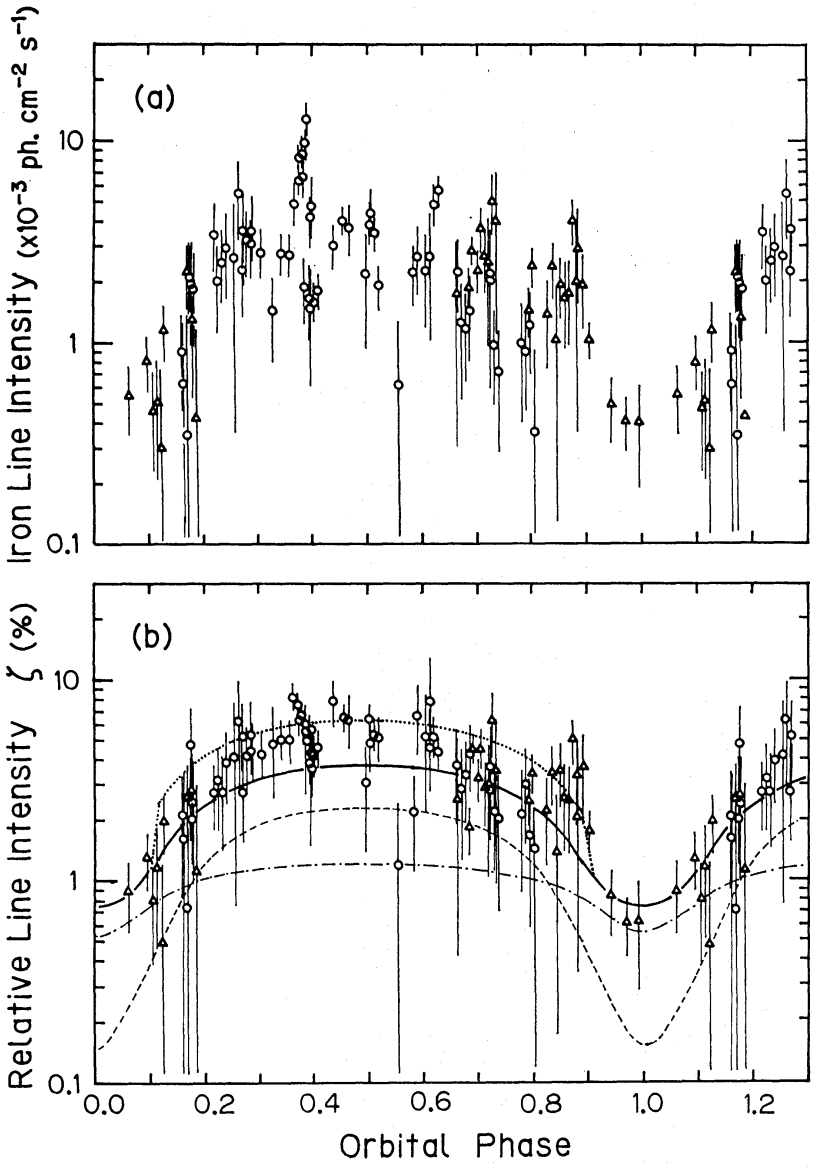

Fig. 7. (a) The observed iron line intensity and (b) the relative line intensity, ζ, as functions of the orbital phase. The thin dashed and dash-dotted curves represent the fractions of the relative line intensity attributed to the stellar atmosphere and to the stellar wind, respectively, and the thick solid curve is their sum. These are calculated on the basis of our model of stellar wind and atmosphere (see text). The dotted curve indicates the intensity including the contribution of fluorescence in the proximity of the neutron star.

line intensity shown in figure 7a.

Several estimates have been presented for the iron K-shell fluorescence line produced in the stellar atmosphere and the stellar wind illuminated by X-rays from the neutron star (Hatchett and McCray 1977; Hatchett and Weaver 1977; Basko 1978). We calculated the orbital phase dependence of the fluorescence iron-line intensity in the Vela X-1/HD 77581 system using the parameters of the stellar wind and the stellar atmosphere obtained in section 3.1. In the calculation we assumed, for simplicity, that iron is neutral with the cosmic abundance ($N_{\rm Fe}=3.8\times10^{-5}N_{\rm H}$ from paper I),

© Astronomical Society of Japan • Provided by the NASA Astrophysics Data System

1986PASJ...38..731S

that the system inclination is $i \simeq 90°$, and that the orbital eccentricity is negligible ($e=0$). The effect of scattering is also neglected, which is justified by the observed low-continuum flux during the eclipse. We also assumed a photon power spectrum with an index $\alpha=1.2$, a cutoff energy $E_c=15$ keV, and an e-folding energy $E_f=30$ keV for the continuum spectrum emitted from the X-ray source, based on the average of the spectra observed during the noneclipse phase. A fluorescence yield of the iron Kα line of $\omega_K=0.34$ and a K-shell absorption edge of $E_K=7.25$ keV are adopted. The parameters $H=2.7\times10^{11}$ cm, $\rho_0=5.6\times10^{-12}$ g cm^{-3}, and $\dot{M}_*=2.4\times10^{-6}\ M_\odot$ yr^{-1} derived in section 3.1 are used for the model of the stellar atmosphere and the stellar wind.

The relative line intensity ζ thus calculated is shown in figure 7b by the solid curve. Here the orbital phase dependence arises solely due to geometrical effects, namely that a variable portion of the reprocessing region is obscured by the companion. About 70% of the calculated ζ at $\Phi_{orb}=0.5$ originates from the stellar atmosphere, whereas more than 80% of ζ at mid-eclipse originates from the stellar wind. The fractions attributed to the stellar atmosphere and the stellar wind are drawn by the thin dashed and thin dash-dotted curves, respectively in figure 7b. From the comparison of the calculated intensity with the observed one, we find that (1) the intensity of iron line during the eclipse phase can be explained by the above model as seen at phase $\Phi_{orb}=0.9$–1.1, (2) the orbital phase dependence with a broad peak at $\Phi_{orb}\simeq0.5$ is well simulated, (3) the data points scatter considerably about the calculated curve but lie mostly above the curve, and (4) the observed phase dependence at the phases just before ingress and after egress is steeper than the calculated one.

The calculated ratio of the maximum relative intensity ζ_{max} at $\Phi_{orb}=0.5$ to the minimum ζ_{min} at $\Phi_{orb}=0.0$ is $(\zeta_{max}/\zeta_{min})_{cal}=5.2$, which is significantly smaller than the observed ratio $(\zeta_{max}/\zeta_{min})_{obs}\simeq8$. The observed value around $\Phi_{orb}\simeq0.5$ is on the average $\zeta_{0.5}\simeq6\%$, contrary to the maximum value of $\zeta_{max}=3.7\%$ expected from the present model. The excess of $\sim2.5\%$ in the relative line intensity corresponds to an equivalent width of about 50 eV. Since a systematic deviation is seen between the intensities observed at $\Phi=0.65$–0.8 in March 1983 and in March 1984, one would suspect that the change of the stellar wind density could be responsible for the fluctuations in the line intensity. A mass-loss rate of $\dot{M}_*\simeq5\times10^{-6}\ M_\odot$ yr^{-1} is an upper limit to explain the intensity at an eclipse, but not enough to explain the noneclipse intensity as seen in the figure. It is also unlikely that the density of the stationary stellar wind changes abruptly by several factors in coincidence with the immersion of the X-ray source.

Some additional reprocessing sites which are completely obscured by the companion star during eclipse are required to explain the excess in ζ during the noneclipse phase. The three following candidates are considered to be additional reprocessing sites: (A) accretion matter trapped in the Alfvén shell of the neutron star, (B) stellar wind matter stagnated around the shock front or the ionization front, and (C) stellar wind matter condensed in the accretion wake behind the neutron star.

Ohashi et al. (1984) suggested the matter trapped in the magnetosphere of the neutron star as a possible origin of the iron Kα fluorescence line. As the electron temperature at the Alfvén shell is considered to be $T_e>10^6$ K and the ionization degree

© Astronomical Society of Japan • Provided by the NASA Astrophysics Data System

1986PASJ...38..731S

is estimated to be predominantly Fe XXIV or higher (Basko 1980), emission lines at 6.7–6.9 keV are expected to be dominant. Hence a question arises whether a sufficient amount of cool matter to explain the observed excess emissions of the 6.4-keV iron line could be accumulated in the Alfvén shell. Hayakawa (1985) and Inoue (1985) discussed the conditions that the matter density above the polar cap and in the Alfvén shell could be high enough to hold a sufficient amount of matter with low degrees of ionization.

In paper I we showed the temporal appearance of inhomogenous clumped regions surrounding the neutron star, accompanying the enhancement of the iron line intensity. A stagnated region of matter will be formed inside the shock front (Fransson and Fabian 1980) or the ionization front (Hatchett et al. 1976; Kallman and McCray 1982) caused by thermal instability. If clumped blobs with an average column density of $\langle N_{\rm H}\rangle \simeq 4\times 10^{22}$ cm^{-2} surround the neutron star spherically, such blobs will additionally produce the fluorescence iron line with an equivalent width of $\sim$40 eV.

In the previous section we also confirmed the existence of the accretion wake with a column density of $N_{\rm H}\simeq 1\times 10^{23}$ cm^{-2} in the second half of the orbital phase. However, the relative line intensity does not increase as much with the orbital phase from $\Phi_{\rm orb}\simeq 0.25$ to $\Phi_{\rm orb}\simeq 0.8$ as is expected from the increase of $N_{\rm H}$ seen in figure 5. The solid angle covered by the accretion wake is estimated to be less than one tenth of a sphere. Nevertheless, the value of ζ for $\Phi_{\rm orb}=0.8$–0.9 larger than that for $\Phi_{\rm orb}=0.1$–0.2 may be due partly to the effect of the accretion wake.

Except for this iron line enhancement at $\Phi_{\rm orb}=0.8$–0.9, the systematic excess of the iron line intensity observed over the calculated intensity is considered to arise from a reprocessing site rather close to the neutron star. In figure 7b we draw a dotted curve, if the excess component near the eclipse behaves in the same way as the continuum shown in figure 1b, assuming the average column density of $\langle N_{\rm H}\rangle = 4\times 10^{22}$ cm^{-2}. A rough agreement with the observed behavior indicates that there is an additional reprocessing site located within $H\simeq 3\times 10^{11}$ cm from the neutron star, thus supporting the possibilities (A) and/or (B).

A comment is made on the sudden disappearance of the X-ray emission observed on March 12, 1983 (Inoue et al. 1984). Hayakawa (1984) suggested the occultation by a small solid body like a planet. If this is the case, the iron line intensity would decrease at most by a factor of about two, since the iron line produced in the stellar atmosphere and the stellar wind should survive. The fact that both the iron line and continuum intensities decreased by the same factor of about ten (Inoue et al. 1984) indicates that Hayakawa's (1984) suggestion is untenable. It is more likely that the sudden intensity drop was caused by a sudden interruption of matter accretion onto the neutron star.

3.3. *Energy Spectra during Eclipse*

At mid-eclipse, the region within a radial distance of 2×10^{12} cm from the X-ray star is obscured by the companion star (HD 77581). Therefore, both the continuum and the line emissions observed during an eclipse (figures 3 IV and V) would be secondary emissions reprocessed in the stellar wind far from the neutron star. This secondary emission includes Thomson scattering which is almost energy inde-

© Astronomical Society of Japan • Provided by the NASA Astrophysics Data System

1986PASJ...38..731S

pendent, and fluorescent line emissions from various elements. Although the stellar atmosphere of the companion is considered to expand up to the scale height of $H \simeq 0.14 R_*$ and the column density of matter across the atmosphere is as large as $N_H \simeq 10^{23}$–10^{24} cm^{-2}, as discussed in section 3.1, the solid angle from the neutron star covered by this stellar ring is only $\delta\Omega/4\pi \simeq 0.016$. On the other hand, the stellar wind with the average column density of $\langle N_H \rangle \simeq 2 \times 10^{22}$ cm^{-2} extends over nearly 4π steradians except the region obscured by the companion star and scatters the X-rays emitted from the source. Considering such a geometry and the scattering cross section of $\sigma_{scatt} \simeq 0.66 \times 10^{-24}$ cm^2 which is almost independent of energy, we can estimate the contribution by continuum X-rays scattered by the stellar atmosphere and the stellar wind to be respectively $\lesssim 1\%$ and $\sim 2\%$ of the X-rays emitted from the X-ray source. Hence the contribution of the stellar ring to the X-ray scattering seems relatively small compared with that of the stellar wind. The total flux of X-rays scattered by the stellar atmosphere and by the stellar wind thus estimated is 2–3% of that emitted from the X-ray source, which is consistent with the observed ratio of the continuum X-ray flux during eclipse to that during the noneclipse phase. The scattered X-ray spectrum should have a similar feature to that during noneclipse phase just after the

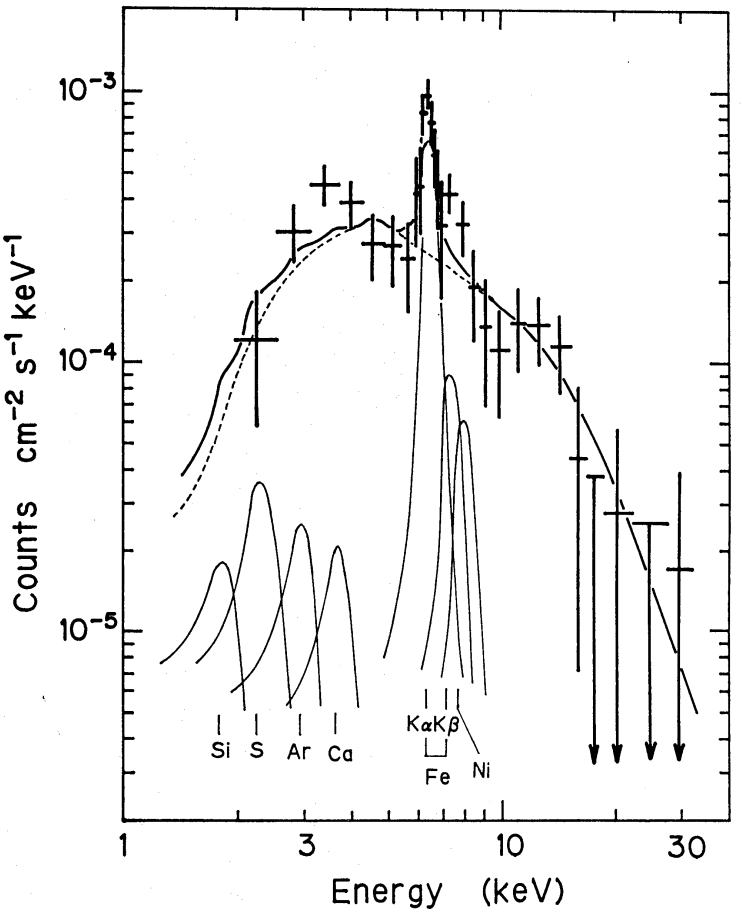

Fig. 8. The X-ray spectrum of Vela X-1 during eclipse (IV plus V of figure 3) compared with the calculated spectrum (thick solid curve). The calculated spectrum is the sum of those expected from the scattering continuum (dashed curve) and the fluoresced lines (thin solid curves).

© Astronomical Society of Japan • Provided by the NASA Astrophysics Data System

1986PASJ...38..731S

egress (e.g., spectrum X in figure 3) with a degraded intensity, because the column density of the stellar wind is a few times 10^{22} cm^{-2} and the scattering cross section is almost independent of energy. The scattered continuum spectrum expected for the above geometry is shown by dashed curves in figure 8 superposed on the observed spectrum.

In contrast to scattering, reprocessing of the fluorescence iron line is more effective, because the photoabsorption cross section at $\sim$7 keV is by a factor of $\sim$3 larger than the scattering cross section. The stellar atmosphere also plays an appreciable role in reprocessing the fluorescence line, although the stellar wind dominates to fluoresce the iron line as discussed in section 3.2. As a result, the iron Kα emission line becomes dominant as seen in figures 3a-IV, 3b-V, and 8. As the iron Kα line is so conspicuous, one might suspect the contributions of other fluorescence lines, such as Kα lines of Si, S, Ar, Ca, and Ni and a Kβ line of iron. In figure 8, we composed the contribution of such lines expected during an eclipse based on the observed intensity of iron Kα line and the matter configuration discussed above. In the calculation, the intensities of Si Kα, S Kα, Ar Kα, Ca Kα, Ni Kα, and iron Kβ lines are respectively estimated to be 7.4%, 7.3%, 3.2%, 2.3%, 6.5%, and 10% of the iron Kα line intensity, taking into account the cosmic abundances and the fluorescence yields of these elements (note that the absorption effects are also taken into account for the emission lines depicted in figure 8). The intensities of these lines are also shown in figure 8 by thin solid curves, indicating minor contributions of these lines except that of the iron Kα line. The resulting spectrum taking into account both the scattering continuum and fluorescence lines explains well the observed spectrum.

The authors are grateful to all the other members of the Tenma team, particularly to H. Kunieda, Y. Tawara, T. Hirano, and T. Kii for useful comments and discussions. Thanks are due to Professor R. Kajikawa and his colleagues in the high-energy physics group of Nagoya University for the use of their high-performance computer FACOM M-200. One of the authors (N.S.) would like to acknowledge a fellowship awarded by the Toyota Physico-Chemical Research Institute.

References

Basko, M. M. 1978, *Astrophys. J.*, **223**, 268.
Basko, M. M. 1980, *Astron. Astrophys.*, **87**, 330.
Bautz, M., Howe, S., Gorecki, A., Lang, F., Levine, A., Primini, F., and Lewin, W. H. G. 1983, *Astrophys. J.*, **266**, 794.
Becker, R. H., Rothschild, R. E., Boldt, E. A., Holt, S. S., Pravdo, S. H., Serlemitsos, P. J., and Swank, J. H. 1978, *Astrophys. J.*, **221**, 912.
Boynton, P. E., Deeter, J. E., Lamb, F. K., Zylstra, G., Pravdo, S. H., White, N. E., Wood, K. S., and Yentis, D. J. 1984, *Astrophys. J. Letters*, **283**, L 53.
Boynton, P. E., Deeter, J. E., Lamb, F. K., and Zylstra, G. 1986, *Astrophys. J.*, **307**, 545.
Castor, J. I., Abbott, D. C., and Klein, R. I. 1975, *Astrophys. J.*, **195**, 157.
Clark, G. W., and Minato, J. R. 1985, in *Japan-US Seminar on Galactic and Extragalactic Compact X-Ray Sources*, ed. Y. Tanaka and W. H. G. Lewin (Institute of Space and Astronautical Science, Tokyo), p. 41.
Conti, P. S. 1978, *Astron. Astrophys.*, **63**, 225.

© Astronomical Society of Japan • Provided by the NASA Astrophysics Data System

1986PASJ...38..731S

Dupree, A. K., Gursky, H., Black, J. H., Davis, R. J., Hartmann, L., Matilsky, T., Raymond, J. C., Hammerschlag-Hensberge, G., van den Heuvel, E. P. J., Burger, M., Lamers, H. J. G. L. M., Vanden Bout, P. A., Morton, D. C., de Loore, C., van Dessel, E. L., Menzies, J. W., Whitelock, P. A., Watson, M., Sanford, P. W., and Pollard, G. S. G. 1980, *Astrophys. J.*, **238**, 969.

Forman, W., Jones, C., Tananbaum, H., Gursky, H., Kellogg, E., and Giacconi, R. 1973, *Astrophys. J. Letters*, **182**, L103.

Fransson, C., and Fabian, A. C. 1980, *Astron. Astrophys.*, **87**, 102.

Friend, D. B., and Castor, J. I. 1982, *Astrophys. J.*, **261**, 293.

Hatchett, S., Buff, J., and McCray, R. 1976, *Astrophys. J.*, **206**, 847.

Hatchett, S., and McCray, R. 1977, *Astrophys. J.*, **211**, 552.

Hatchett, S., and Weaver, R. 1977, *Astrophys. J.*, **215**, 285.

Hayakawa, S. 1984, *Adv. Space Res.*, **3**, Nos. 10–12, 35.

Hayakawa, S. 1985, *Phys. Rep.*, **121**, 317.

Inoue, H. 1985, *Space Sci. Rev.*, **40**, 317.

Inoue, H., Ogawara, Y., Ohashi, T., Waki, I., Hayakawa, S., Kunieda, H., Nagase, F., and Tsunemi, H. 1984, *Publ. Astron. Soc. Japan*, **36**, 709.

Joss, P. C., and Rappaport, S. A. 1984, *Ann. Rev. Astron. Astrophys.*, **22**, 537.

Kallman, T. R., and McCray, R. 1982, *Astrophys. J. Suppl.*, **50**, 263.

Koyama, K., Ikegami, T., Inoue, H., Kawai, N., Makishima, K., Matsuoka, M., Mitsuda, K., Murakami, T., Ogawara, Y., Ohashi, T., Suzuki, K., Tanaka, Y., Waki, I., and Fenimore, E. E. 1984, *Publ. Astron. Soc. Japan*, **36**, 659.

McClintock, J. E., Rappaport, S., Joss, P. C., Bradt, H., Buff, J., Clark, G. W., Hearn, D., Lewin, W. H. G., Matilsky, T., Mayer, W., and Primini, F. 1976, *Astrophys. J. Letters*, **206**, L99.

McCray, R., Kallman, T. R., Castor, J. I., and Olson, G. L. 1984, *Astrophys. J.*, **282**, 245.

Morrison, R., and McCammon, D. 1983, *Astrophys. J.*, **270**, 119.

Nagase, F., Hayakawa, S., Kii, T., Sato, N., Ikegami, T., Kawai, N., Makishima, K., Matsuoka, M., Mitani, K., Murakami, T., Oda, M., Ohashi, T., Tanaka, Y., and Kitamoto, S. 1984a, *Publ. Astron. Soc. Japan*, **36**, 667.

Nagase, F., Hayakawa, S., Kunieda, H., Masai, K., Sato, N., Tawara, Y., Inoue, H., Koyama, K., Makino, F., Makishima, K., Matsuoka, M., Murakami, T., Oda, M., Ogawara, Y., Ohashi, T., Shibazaki, N., Tanaka, Y., Miyamoto, S., Tsunemi, H., Yamashita, K., and Kondo, I. 1984b, *Astrophys. J.*, **280**, 259.

Nagase, F., Hayakawa, S., Makino, F., Sato, N., and Makishima, K. 1983, *Publ. Astron. Soc. Japan*, **35**, 47.

Nagase, F., Hayakawa, S., Sato, N., Masai, K., and Inoue, H. 1986, *Publ. Astron. Soc. Japan*, **38**, 547 (paper I).

Ohashi, T., Inoue, H., Koyama, K., Makino, F., Matsuoka, M., Suzuki, K., Tanaka, Y., Hayakawa, S., Tsunemi, H., and Yamashita, K. 1984, *Publ. Astron. Soc. Japan*, **36**, 699.

Rappaport, S., Joss, P. C., and McClintock, J. E. 1976, *Astrophys. J. Letters*, **206**, L103.

Rappaport, S., Joss, P. C., and Stothers, R. 1980, *Astrophys. J.*, **235**, 570.

Sadakane, K., Hirata, R., Jugaku, J., Kondo, Y., Matsuoka, M., Tanaka, Y., and Hammerschlag-Hensberge, G. 1985, *Astrophys. J.*, **288**, 284.

Tanaka, Y., Fujii, M., Inoue, H., Kawai, N., Koyama, K., Maejima, Y., Makino, F., Makishima, K., Matsuoka, M., Mitsuda, K., Murakami, T., Nishimura, J., Oda, M., Ogawara, Y., Ohashi, T., Shibazaki, N., Suzuki, K., Waki, I., Yamagami, T., Kondo, I., Murakami, H., Hayakawa, S., Hirano, T., Kunieda, H., Masai, K., Nagase, F., Sato, N., Tawara, Y., Kitamoto, S., Miyamoto, S., Tsunemi, H., Yamashita, K., and Nakagawa, M. 1984, *Publ. Astron. Soc. Japan*, **36**, 641.

van der Klis, M., and Bonnet-Bidaud, J. M. 1984, *Astron. Astrophys.*, **135**, 155.

van Genderen, A. M. 1981, *Astron. Astrophys.*, **96**, 82.

van Paradijs, J., Zuiderwijk, E. J., Takens, R. J., Hammerschlag-Hensberge, G., van den Heuvel, E. P. J., and de Loore, C. 1977, *Astron. Astrophys. Suppl.*, **30**, 195.

Watson, M. G., and Griffiths, R. E. 1977, *Monthly Notices Roy. Astron. Soc.*, **178**, 513.

White, N. E., Swank, J. H., and Holt, S. S. 1983, *Astrophys. J.*, **270**, 711.

© Astronomical Society of Japan • Provided by the NASA Astrophysics Data System